Contents lists available at SciVerse ScienceDirect

Comptes Rendus Mecanique

www.sciencedirect.com

A second gradient continuum model accounting for some effects of micro-structure on reconstructed bone remodelling

Angela Madeo [a,e,*], D. George [c], T. Lekszycki [b,d,e], Mathieu Nierenberger [c], Yves Rémond [c,e]

[a] LGCIE, université de Lyon, INSA, 20, avenue Albert-Einstein, 69621 Villeurbanne cedex, France
[b] Department of Machinery Design and Biomedical Engineering, Warsaw University of Technology, 85 Narbutta Street, 02-524 Warsaw, Poland
[c] IMFS, université de Strasbourg, CNRS, 2, rue Boussingault, 67000 Strasbourg, France
[d] Warsaw Medical University, 4 Lindleya Street, 02-005 Warsaw, Poland
[e] International Research Center M&MOCS, University of L'Aquila, Cisterna di Latina, Italy

ARTICLE INFO

ABSTRACT

We propose a second gradient, two-solids, continuum mixture model with variable masses to describe the effect of micro-structure on mechanically-driven remodelling of bones grafted with bio-resorbable materials. A one-dimensional numerical simulation is addressed showing the potentialities of the proposed generalized continuum model. In particular, we show that the used second gradient model allows for the description of some micro-structure-related size effects which are known to be important in hierarchically heterogeneous materials like reconstructed bones. Moreover, the influence of the introduced second gradient parameters on the final percentages of replacement of artificial bio-material with natural bone tissue is presented and discussed.

1. Introduction

It is nowadays well established in scientific literature that interactions between mechanics and biology are crucial to correctly interpret and describe the behavior of growing tissues (see e.g. [1–4]). This is strictly related to the fact that Nature has developed "optimization methods" which, given the applied external loads, allow to obtain a proper resistance against mechanical failure with a minimum use of material. Since the external applied loads unceasingly vary during life, living tissues must continuously be resorbed and synthesized in order to be able to resist to the actual loads with the minimum possible quantity of matter. The functional adaptation of bone to mechanical usage implies the existence of a physiological control process (see e.g. [5–7]). Essential components for the control process include sensors for detecting mechanical usage and transducers to convert the usage measures to cellular responses. The cellular responses lead to gradual changes in bone shape and/or material properties and, once the structure has adapted sufficiently, the feedback signal is diminished and further changes to shape and properties are stopped. Although the just presented description of biological phenomena occurring in growing tissues is certainly incomplete, it includes a number of processes which are definitely relevant when the observed mechanical adaptation takes place.

* Corresponding author at: LGCIE, université de Lyon, INSA, 20, avenue Albert-Einstein, 69621 Villeurbanne cedex, France.
E-mail addresses: angela.madeo@insa-lyon.fr (A. Madeo), george@unistra.fr (D. George), tlekszyc@ippt.gov.pl (T. Lekszycki), mathieu.nierenberger@etu.unistra.fr (M. Nierenberger), remond@imfs.u-strasbg.fr (Y. Rémond).

The amazing problem of bone adaptation and remodeling stimulated the minds of biologists and mechanicians ever since 1892 when Wolff (see [8], and [9]) observed that "internal architecture and external conformation of bones changes in accordance with mathematical laws". The twentieth century has then seen an explosion of the research in the field and different mathematical models have been proposed to describe functional adaptation and bone remodelling (see e.g. [10,11]).

It is nowadays well established that the cells which are involved in functional adaptation of bone are divided in two main big classes: (i) the sensor cells (or osteocytes) which are able to detect the external mechanical stimulus and to transduce it in a suitable biological signal which can be decoded by other cells, and (ii) the actor cells (osteoblasts and osteoclasts) which detect the signal emitted by the osteocytes and respectively synthesize and resorb bone tissue depending on the state of mechanical excitation. Various mechanical stimuli have been proposed as triggers for bone adaptation, including strain (see [12]) strain energy density (see e.g. [3,4,13,14]), tissue damage (see [15]), daily stress stimulus (see [1]) and different forms of effective stress (see [16]). In this article we follow the idea of adopting the strain energy density (SED) as the principal trigger of bone remodeling. More precisely, we assume that the osteocytes are well placed within bone porosity to function as "strain gauges", and to emit a signal (stimulus) the intensity of which is proportional to the measured strain energy and to bone apparent density. Moreover, we assume that a threshold value of the stimulus exists such that osteoblasts (bone synthesis) are activated if the value of stimulus is higher than this threshold, while osteoclasts (bone resorption) are activated if the value of stimulus is lower than the threshold itself. The hypothesis of existence of such a threshold value is based on the idea that a high value of the deformation energy is associated to a need of a more compact bone, while a low value of strain energy may be associated to a "surplus" of material at a given location which can then be resorbed and reused in other locations subjected to higher mechanical solicitations. The idea of using SED as the principal trigger of bone remodeling is well known in the scientific literature and has been validated by several experimental observations (see e.g. [3]).

The understanding of the profound interactions between mechanics and biology in functional bone adaptation and re-modeling naturally led to the production and current use in medical practice of artificial bio-resorbable scaffolds which initially have the function of sustaining external mechanical loads, but are progressively resorbed by osteoclasts and partially or completely replaced by natural bone tissue (see e.g. [17–20]). Bio-resorbable materials are more and more used in bone reconstructive surgery and represent a good alternative to more classical materials (see e.g. [21–25]) which more drastically interact with the organism especially in the long period (see e.g. [26–28]). Indeed, we want to stress the fact two big classes of bio-materials can be generally distinguished: bio-resorbable and bio-degradable. The first ones (as those based on hydroxyapatite, see e.g. [29] and [19]) are mostly processed by the osteoclasts while the second ones (as different polymers, see e.g. [30] and [31]) are mainly resorbed in the process of hydrolysis. In practice, both processes always coexist and, depending on the constitution of the graft, one process or the other results to be dominant. To the sake of completeness, both processes (resorption by osteoclasts and degradation by hydrolysis) should be included in one single formulation but, as a first step, we want to focus separately on each of them to make clear their understanding. Since more work is done in the literature on bio-degradable materials (see e.g. [30] and [31]), we start considering in this paper bio-resorbable ones and we will complete our formulation in future work including the effect of bio-degradation.

While continuum models for the description of natural bone regeneration are widely spread in the scientific literature (see among many others [32–35,12]), the conception of rigorous models allowing for the description of bio-materials re-sorption and of their gradual replacement by natural bone tissue is still an open challenge. One of the main objectives of this paper is, following what done in [4], to introduce an innovative continuum mixture model which allows for describing phenomena of natural bone remodeling on one hand and, on the other hand, phenomena of resorption of bio-resorbable artificial materials followed by a gradual substitution with natural bone tissue. A model of this type would be of interest for the optimal design of bio-resorbable prostheses currently used in bone reconstructive surgery. Indeed, the use of a macroscopic continuum model does not explicitly allow to account for the precise micro-structure of the scaffold, i.e. for the geometric distribution of porosity and the size of the pores inside the Representative Elementary Volumes. Nevertheless, an averaged porosity is accounted for in the present model and a precise constitutive form for this parameter in terms of the apparent density of the constituents is given in the body of the paper. In order to explicitly take into account for the precise porosity patterns inside the scaffold some homogenization procedures should be used of the type presented e.g. in [36] and [37].

The continuum mixture theory developed here will also take into account the possibility of describing the effect of micro-structure on the overall mechanical behavior of both bone and bio-materials by means of the use of a second gradient approach which has been widely recognized to be useful for these purposes. It is indeed well established in scientific literature (see e.g. [38–42]) that classical Cauchy-type continuum theories do not allow for the correct prediction of the mechanical behavior of bone, when considering sufficiently small scales and/or particular loading conditions. These scale effects are related to the fact that bone is a hierarchically heterogeneous material, i.e. it can be considered as homogeneous at the scale of the millimeter, but it starts presenting heterogeneities at the scale of the micron (see e.g. [43,44]) and even at lower scales (see e.g. [45]). Indeed, at this scale quasi-periodic circular structures (osteons) can be detected which confer highly heterogeneous properties to the material itself. It is for this reason that classical continuum theory does not allow to describe the correct behavior of bone at such small scales where the prediction made by Cauchy continuum theory starts being far away from the experimental evidence. In [38] a clear presentation of some size effects observed in bone is given and explained by means of experimental evidences. The authors explain how these size effects can be accounted for by

using a Cosserat-type continuum theory which allows to perform much more precise predictions. The fact of modelling the mechanical behavior of bone by means of Cosserat-type theories is well established in the scientific literature as shown by the numerous theoretical and experimental publications on this subject (see e.g. [38,46–48]).

The idea which is developed in this article is to account for the discussed size effects by using a second gradient continuum theory (see also [49]) instead of a Cosserat-type theory which needs the introduction of a more complicated kinematics accounting for micro-rotations. A second gradient theory allows for the description of some microscopic features of the considered material, even if remaining in the framework of macroscopic continuum theories (see among many others [50]) and is able to correctly describe a considerable number of the cited size effects (see e.g. [51,52]). Indeed, second gradient theories permit to obtain a generalization of classical Cauchy continuum theory in the sense that they introduce the possibility of considering the existence of particular internal contact actions exchanged between sub-bodies of the continuum which are more general than those considered in classical first gradient theories (see [53–59,81]). In particular, while in classical continuum theories only forces per unit area proportional to the normal to the Cauchy cut are described, in second gradient theories one has the possibility to introduce more complicated contact actions which depend e.g. on the curvature of the Cauchy cut (so-called "double forces" following the nomenclature adopted by Germain in [53]). As an example, we can say that second gradient theories allow for the description of couples per unit area exchanged between sub-bodies of the continuum, while classical theories do not. Such a possibility of describing more complicated contact actions allows for the description of some mechanical responses of the continuum which are directly related to its micro-structure (see e.g. [50]).

The proposed second gradient continuum mixture model is finally applied to a simple one-dimensional case in which natural bone and bio-resorbable material are originally separated by a material discontinuity surface. A tensile external load is applied to the considered specimen and the effect of the introduced second gradient parameters on the final percentage of replacement of artificial bio-material with natural bone tissue is investigated. The presented preliminary results show how the introduced second gradient model allows for describing some scale effects which are directly related to bone and bio-material micro-structure. Since it aims to describe extremely complicated bio-mechanical phenomena, the presented model introduces a large number of biological and mechanical parameters which therefore need to be carefully analyzed. A rigorous parametric study will be performed in a subsequent paper in order to study the influence of each of these parameters on the overall process of reconstructed bone remodelling. Particular attention will be paid to the effect of the second gradient parameters on the final percentage of replacement of artificial bio-material with natural bone tissue.

2. Equilibrium equations for a second gradient two-solids mixture accounting for mass creation and dissolution as driven by bio-mechanical coupling

In this section we start by introducing the mechanical equations suitable for describing the deformation of a second gradient continuum. We will then propose a set of ordinary differential equations accounting for phenomena of creation and dissolution of mass as driven by the coupling between the external mechanical excitation and the resulting biological stimulus. The proposed set of mechanical and biological equations will be proven to be suitable for describing remodelling phenomena in reconstructed bone as well as some scale effects related to the heterogeneous micro-structure of both bone and bio-material.

2.1. Second gradient equilibrium equations

Following standard procedures of mixture theory (see e.g. [60]), we describe the deformation of a two-solids continuum mixture by introducing a Lagrangian (or reference) configuration $B_L \subset \mathbb{R}^3$ and a suitably regular kinematical field $\chi(\mathbf{X}, t)$ which associates to any material point $\mathbf{X} \in B_L$ its current position $\mathbf{x}$ at time t. The kinematics of the system is completed by introducing two Lagrangian densities $\rho_b^*(\mathbf{X}, t)$ and $\rho_m^*(\mathbf{X}, t)$ which represent the density of the natural bone tissue and of the artificial material respectively. We explicitly remark that, in our mixture model, we associate to each material particle $\mathbf{X}$ two different densities which can evolve with time. The image of the function χ gives, at any instant t, the current shape of the body $B_E(t)$: this time-varying domain is usually referred to as the Eulerian configuration of the mixture and, indeed, it represents the system during its deformation. Since we will use it in the following, we also introduce the displacement field[1] $\mathbf{u}(\mathbf{X}, t) := \chi(\mathbf{X}, t) - \mathbf{X}$, the tensor $\mathbf{F} := \nabla\chi$ and the Green–Lagrange deformation tensor $\boldsymbol{\varepsilon} := (\mathbf{F}^T \cdot \mathbf{F} - \mathbf{I})/2$.

Let $U^*(\boldsymbol{\varepsilon}, \nabla\boldsymbol{\varepsilon}, \rho_b^*, \rho_m^*)$ be the strain energy of a second gradient continuum mixture which is assumed to depend on the Green–Lagrange deformation tensor ε, on its gradient and also on the Lagrangian apparent mass densities of both bone and bio-material. It can be shown by means of a variational principle (see e.g. the methods presented in [61]) that, neglecting external body forces, the bulk equilibrium equation for such a system reads

$$div\left[\mathbf{F} \cdot \left(\frac{\partial U^*}{\partial \boldsymbol{\varepsilon}} - div\left(\frac{\partial U^*}{\partial \nabla\boldsymbol{\varepsilon}} \right) \right) \right] = 0 \tag{1}$$

---

[1] Here and in the sequel the symbol := will be used when we want to indicate the definition of a new quantity.

together with the following duality conditions valid on any discontinuity surface $\Sigma \subset B_L$ of such a continuum

$$\left[\left|\mathbf{t} \cdot \delta\mathbf{u}\right|\right] = 0, \qquad \left[\left|\boldsymbol{\tau} \cdot (\delta\mathbf{u})_n\right|\right] = 0, \qquad \left[\left|\mathbf{f} \cdot \delta\mathbf{u}\right|\right] = 0 \tag{2}$$

The first two of these conditions are valid on Σ while the last one is valid on the edges $\mathcal{E}$ of Σ, if any. In the previous formulas we set

$$\mathbf{t} := \left[\mathbf{F} \cdot \left(\frac{\partial U^*}{\partial \boldsymbol{\varepsilon}} - div\left(\frac{\partial U^*}{\partial \nabla \boldsymbol{\varepsilon}}\right)\right)\right] \cdot \mathbf{n} - div^\Sigma \left(\mathbf{F} \cdot \frac{\partial U^*}{\partial \nabla \boldsymbol{\varepsilon}} \cdot \mathbf{n}\right) \tag{3}$$

$$\boldsymbol{\tau} := \left(\mathbf{F} \cdot \frac{\partial U^*}{\partial \nabla \boldsymbol{\varepsilon}} \cdot \mathbf{n}\right) \cdot \mathbf{n}, \qquad \mathbf{f} := \left(\mathbf{F} \cdot \frac{\partial U^*}{\partial \nabla \boldsymbol{\varepsilon}} \cdot \mathbf{n}\right) \cdot \boldsymbol{\nu} \tag{4}$$

where, $\mathbf{n}$ is the unit normal vector to the surface Σ, div^Σ stands for the surface divergence operator on Σ, if the edge is regarded as the border of a surface then $\boldsymbol{\nu}$ is the normal vector to the considered edge which is tangent to the surface, $\delta\mathbf{u}$ is the variation of the displacement field and $(\delta\mathbf{u})_n := \nabla(\delta\mathbf{u}) \cdot \mathbf{n}$ stands for the normal derivative of the variation of the displacement field. Finally, given a quantity a defined everywhere and having continuous traces a^+ and a^- on the two sides of Σ respectively, we have set $[|a|] := a^+ - a^-$ (with a slight abuse of notation, we use the same symbol for the jump across edges).

We explicitly remark that the vector $\mathbf{t}$ represents the so-called "generalized force" which, contrarily to what happens in classical Cauchy theory, explicitly depends on the "shape" of Σ. Moreover, following the notation introduced by Germain [53], the vector $\boldsymbol{\tau}$ is the so-called "double-force", i.e. a special type of non-local contact action which expends power on the normal derivative of velocity. Finally, $\mathbf{f}$ represents a contact action per unit line which can be exchanged by two subbodies of the considered body across the edges (if any) of the Cauchy cut.

2.2. Bone remodelling equations

We now want to formulate a well-posed evolutionary problem for the introduced kinematical fields which is able to catch the most important features of the remodelling processes occurring in bone tissue after initial healing and in presence of bio-resorbable grafts initially functioning as a bone tissue filler and support. Before introducing the differential equations which we believe to be suitable to accomplish this task, we recall here some basic biological facts which led us to use them in our modelling. We can start distinguishing two types of cells (which belong to the common class of so-called "actor cells"), namely the osteoblasts (specialized in new bone tissue formation) and the osteoclasts (which are able to resorb both natural bone and bio-resorbable material). We assume that these two kinds of cells are present everywhere in both the living bone tissue and artificial material under the unique condition that a suitable porosity is present. In other words, we do not consider here those cases in which the bio-resorbable scaffold is so extended that actor cells cannot survive in the first phases after healing due to an insufficient vascularization. The biological equations presented here must therefore be limited to study those cases in which the bio-resorbable grafts are small enough to assure the survival of actor cells also in the inner regions of the scaffold. The activity of osteoblasts and/or osteoclasts is regulated by the instructions of a signal generated by a third kind of cells called osteocytes: this signal is proportional to the deformation which the osteocytes can measure at a given point (for this reason they are also called "sensor cells"). In order to measure deformation energy at a given point, the sensor cells do not move and spend all their life in that point. Sensor cells originate from osteoblasts when these latter have accomplished their task of synthesizing new bone around them: when an osteoblast is completely surrounded by new natural bone tissue it changes its nature and becomes an osteocyte, i.e. a sensor cell which starts to measure deformation and to emit a signal proportional to its measured value. This brief and simplified description of the biology which is known to take place behind the process of reconstructed bone remodelling is sufficient to justify the remodelling equations which we choose to use in this paper. For a more detailed description of the biological phenomena occurring in natural bone and artificial bio-resorbable material remodelling we refer to [4]. Given the just described coupled biological and mechanical phenomena, we are now able to postulate a proper set of differential equations which are able to catch the main features of the described bio-mechanical phenomena. We choose the evolutionary equations for apparent densities to be simply first order ordinary differential equations with respect to time. In formulas, we assume that

$$\frac{\partial \rho_b^*}{\partial t} = \mathcal{A}_b(\varphi^*, S^*), \qquad \frac{\partial \rho_m^*}{\partial t} = \mathcal{A}_m(\varphi^*, S^*) \tag{5}$$

where φ^* is the porosity of the considered continuum mixture and S^* is the biological stimulus. We will duly explain in the following how the porosity φ^* and the stimulus S^* are assumed to constitutively depend on the introduced basic kinematical fields.

These equations are similar to those studied, among others, in [62–65]. However, the analysis which lead to the "bifurcation chart" in Fig. 4 of [62] cannot be easily repeated here since the study of bifurcation in the presented instance should account for the possible variations of resorption and synthesis parameters, which indeed dramatically influence the final form and structure of reconstructed bone.

As already remarked, the remodelling-constitutive equations for $\mathcal{A}_b$ and $\mathcal{A}_m$ must account for different phenomena of biological and mechanical nature and for some geometrical circumstances: (i) the surface available for resorption or

synthesis "inside" the considered macroscopic material particle depends on the "effective" porosity field; (ii) the different properties of bone tissue and bio-material determine different resorption rates, due to the different effect of actor cells on these different material; (iii) a positive stimulus triggers synthesis of natural bone tissue, while a negative stimulus gives rise to resorption of both natural bone and bio-material.

The previous considerations are consequence of the biological nature of the process of synthesis and resorption: in particular, osteoclasts adsorb at the same time (and presumably they are not able to be completely selective) both the bone-tissue and the resorbable material while osteoblasts produce only bone tissue. In this paper, following what was done in [4], we will assume that

$$\mathcal{A}_b(\varphi^*, S^*) = A_b(S^*)H(\varphi^*), \qquad \mathcal{A}_m(\varphi^*, S^*) = A_m(S^*)H(\varphi^*) \tag{6}$$

where the functions A_b and A_m are piece-wise linear functions with different slopes for negative and positive values of stimulus (remark that, according to assumption (iii), A_m must vanish when $S^* > 0$, as there cannot be synthesis of bio-material) and the function H is designed in order to account for the influence of "effective" porosity on the biological activity of actor cells: when "effective" porosity is too large there is not enough material on which actor cells may deposit, when it is too small there is not enough free space in the pores to allow their mobility and deposit. We choose the shape of H in such a way that $H = 0$ for $\varphi = 0$ or $\varphi = 1$. In particular, the following forms for the functions $H(\varphi)$, A_b and A_m have been chosen to perform numerical simulations:

$$H = k\varphi^*(1 - \varphi^*), \qquad A_b(S^*) = \begin{cases} s_b S^* & \text{for } S^* > 0, \\ r_b S^* & \text{for } S^* < 0, \end{cases} \qquad A_m(S^*) = \begin{cases} 0 & \text{for } S^* > 0 \\ r_m S^* & \text{for } S^* < 0 \end{cases} \tag{7}$$

where k is a suitable constant parameters, s_b and r_b will be called synthesis rate and resorption rate for bone tissue respectively and r_m will be called resorption rate for bio-material.

In order to close the problem, we need to explicitly give the constitutive relationships linking the porosity and the stimulus to the introduced kinematical fields. In what follows we will assume that

$$\varphi^* = 1 - \theta \frac{(\rho_b^* + \rho_m^*)}{\rho_{\max}} \tag{8}$$

$$S^*(\mathbf{X}, t) = \left(\int\limits_{B_L} U^*(\mathbf{X}_0, t) d^*(\mathbf{X}_0, t) \exp\left(-D \left\| \chi(\mathbf{X}) - \chi(\mathbf{X}_0) \right\|\right) d\mathbf{X}_0 \right) - S_0^*(\mathbf{X}, t), \quad d^* = \eta \frac{\rho_b^*}{\rho_{\max}} \tag{9}$$

where $\theta \in [0, 1]$, $\rho_{\max}$ is the density of compact bone (corresponding to minimum porosity), d^* is the fraction of osteocytes (it is assumed to be proportional to ρ_b^* since osteocytes take birth from osteoblasts when they are completely surrounded by bone tissue, hence osteocytes can be present only simultaneously with natural bone), $1/D$ is a length accounting for the range of action of the signal sent by osteocytes, and $\eta \in [0, 1]$. Moreover, S_0^* represents a threshold value for the stimulus which discriminates between resorption and synthesis: indeed if the integral on the right hand side of $(9)_1$ is smaller than S_0^* then the stimulus is negative and resorption takes place, while if it is greater than S_0^* the overall stimulus is positive and synthesis of natural tissue occurs. The evolution equations (5), because of constitutive equations (6) are non-linear and depend on the value of strain energy of the whole body by means of the integral operator (9) which is non-linear as well. The stimulus introduced here describes only some precise characteristics of the network of sensor and "actuator" cells in living bone tissues since it has a rather complex (and not completely known) behavior. The mechanisms of signal transmission occurring in this network would deserve a careful study: indeed, its description would require a modelling procedure which needs ideas and methods extensively employed in an apparently far research field as wave propagation in coupled electromechanical systems (see e.g. [66–68]).

3. A simple one-dimensional, linearized, isotropic, second gradient problem

Let us now consider a Lagrangian reference frame (X, Y, Z). We assume that the displacement vector has only one non-vanishing component along the X axis, i.e. $\mathbf{u}(X, t) = (u(X, t), 0, 0)$. With this assumption and assuming the hypothesis of small displacements (linear case), it is easy to show that

$$\mathbf{F} = \begin{pmatrix} (u' + 1) & 0 & 0 \\ 0 & 1 & 0 \\ 0 & 0 & 1 \end{pmatrix}, \qquad \boldsymbol{\varepsilon} = \frac{1}{2} \begin{pmatrix} u'(u' + 2) & 0 & 0 \\ 0 & 0 & 0 \\ 0 & 0 & 0 \end{pmatrix} \approx \begin{pmatrix} u' & 0 & 0 \\ 0 & 0 & 0 \\ 0 & 0 & 0 \end{pmatrix} \tag{10}$$

where we clearly denote by an apex the partial differentiation with respect to the space variable X.

Let us also consider the following particular quadratic form for second gradient strain energy valid for the isotropic case:

$$U^*(\boldsymbol{\varepsilon}, \nabla\boldsymbol{\varepsilon}, \rho_b^*, \rho_m^*) = \mu(\rho_b^*, \rho_m^*)\boldsymbol{\varepsilon}^2 + \frac{\lambda(\rho_b^*, \rho_m^*)}{2}(tr(\boldsymbol{\varepsilon}))^2 + \frac{\gamma(\rho_b^*, \rho_m^*)}{2}(\nabla tr(\boldsymbol{\varepsilon}))^2 \tag{11}$$

Indeed, it is known that, due to its hierarchical micro-structure, bone often behave as an anisotropic material (see e.g. [69–71]), so that the considered expression for the deformation energy should be generalized to describe such more

complicated cases. The parameter γ is the second gradient elasticity parameter, while λ and μ are the classical Lamé parameters of the mixture which can also be given in terms of the Young modulus E and of the Poisson coefficient ν (see Appendix B).

In the considered one-dimensional case the proposed expression of the strain energy simplifies into

$$U^*\big(y, y', \rho_b^*, \rho_m^*\big) = \frac{1}{2} \frac{E(\rho_b^*, \rho_m^*)}{N} y^2 + \frac{1}{2} \gamma\big(\rho_b^*, \rho_m^*\big)\big(y'\big)^2 \tag{12}$$

where E is the Young modulus of the mixture, ν its Poisson coefficient and where we set $y := u'$, $N := (1 + \nu)(1 - 2\nu)/(1 - \nu)$.

In the example considered, the elasticity parameters are not constant as in classical elasticity, but vary as functions of the apparent mass densities ρ_b^* and ρ_m^*. In particular, we will assume in what follows that the Poisson coefficient remains constant in space and time, while we consider the following forms for the Young modulus and the second gradient parameter

$$E\big(\rho_b^*, \rho_m^*\big) = \left(E_b\left(\frac{\rho_b^*}{\rho_{\max}}\right)^\beta + E_m\left(\frac{\rho_m^*}{\rho_{\max}}\right)^\beta\right), \qquad \gamma\big(\rho_b^*, \rho_m^*\big) = \left(\gamma_b\left(\frac{\rho_b^*}{\rho_{\max}}\right)^\alpha + \gamma_m\left(\frac{\rho_m^*}{\rho_{\max}}\right)^\alpha\right) \tag{13}$$

where all the quantities which have not been introduced before are constants.

3.1. Mechanical equilibrium equation and naturally associated boundary conditions

We want to study the deformation of 1D a second gradient medium of length L clamped at $X = 0$ and subjected to a simple tension $\mathbf{f}^{ext} = (f^{ext}, 0, 0)$ at $X = L$. At $X = L/2$ (in the middle of the specimen) we consider a surface of discontinuity of the material properties (interface between natural bone and artificial material at the initial time) such that the two considered materials are clamped together. We explicitly remark here that the considered discontinuity surface is a material surface for both the constituents (i.e. it is always constituted by the same material particles). Indeed, the continuum model presented here does not account for the possibility of considering discontinuity surfaces which are non-material for one of the considered constituents (as done e.g. in [72]). An approach of this type would be indeed necessary if one wants e.g. to consider a fluid saturating the pores of the considered porous continuum and to impose that the discontinuity surface between natural bone and bio-material is permeable to this fluid. Indeed, the coupling between second gradient porous matrices and compressible saturating fluids would be interesting to be treated extending e.g. the methods presented in [73,74]. This would allow to take into account the effect of the presence of a saturating fluid inside the pores on the overall process of reconstructed bone remodelling.

With the assumptions made for the considered one-dimensional, isotropic case, the bulk equilibrium equation (1) simplifies to

$$\left(\frac{E}{N} y\right)' - \big(\gamma y'\big)'' = 0 \tag{14}$$

An equation of this type governs the motion of the 1D continuum mixture both for $X \in [0, L/2]$ and $X \in [L/2, L]$. We remark that the one-dimensional application presented here does not account for the presence of transversal sections in the considered specimen and only considers a simple tensile external load. Indeed, it would be interesting to test more general geometries and external loading patterns extending e.g. the methods used in [75].

As far as jump conditions are concerned, they must be chosen on the basis of the physics of the problem to be treated and in such a way that the duality conditions (2) are satisfied. For the considered problem, we can say that the generalized clamp at $X = 0$ results in the kinematical conditions $\delta\mathbf{u} = 0$ and $(\delta\mathbf{u})_n = 0$; the internal generalized clamp gives rise to the jump conditions $[|\mathbf{u}|] = 0$, $[|\mathbf{t}|] = 0$, $[|(\delta\mathbf{u})_n|] = 0$ and $[|\boldsymbol{\tau}|] = 0$ in $X = L/2$; finally at the free end $X = L$ the following conditions hold $\mathbf{t} = f^{ext}$ and $\boldsymbol{\tau} = 0$. It is easy to check that all these natural and kinematical conditions are compatible with the first two duality conditions (2). The last of conditions (2) does not intervene here since it holds on the edges of the discontinuity Σ which do not exist since Σ reduces to a point in the considered one-dimensional case. It can be checked, recalling definitions (3) and (4) and the considered isotropic expression for the deformation energy, that in the considered one-dimensional, second gradient, linearized case these boundary conditions simplify into

$$u = 0, \qquad y = 0 \qquad \text{in } X = 0$$
$$[|u|] = 0, \qquad \left[\left|\frac{E}{N} y - \big(\gamma y'\big)'\right|\right] = 0, \qquad [|y|] = 0, \qquad [|\gamma y'|] = 0 \qquad \text{in } X = L/2$$
$$\frac{E}{N} y - \big(\gamma y'\big)' = f^{ext}, \qquad \gamma y' = 0 \qquad \text{in } X = L \tag{15}$$

where we recall that we set $y := u'$. We will limit ourselves to solve the problem in terms of the variable y instead of determining the displacement u since this is sufficient to calculate the strain energy and so the biological stimulus. For

this reason the boundary conditions involving the zero-th order derivative of displacement will not be considered in what follows.

We explicitly remark that Eq. (14) can easily be integrated in both the regions $X > L/2$ and $X < L/2$ and that the integration constant can be determined by using the first of the boundary conditions valid at $X = L$ and the second of the jump conditions valid at $X = L/2$.

We finally note that in the considered 1D case the expression (9) for the stimulus simplifies into

$$S^*(X,t) = \left(\int_0^L U^*(X_0,t) d^*(X_0,t) \exp\left(-D\|\chi(X) - \chi(X_0)\|\right) \mathrm{d}X_0 \right) - S_0^*(X,t) \tag{16}$$

where we recall that the strain energy U^* and the osteocytes fraction d^* are constitutively given in Eqs. (12) and (9)$_2$, respectively.

3.2. Non-dimensional form of mechanical and biological equations

We now want to write all the equations in non-dimensional form. To do so, we start from mechanical equations and we introduce the non-dimensional variables $\tilde{x} = X/L_0$, $\tilde{u} = u/u_0$, $\tilde{E} = E/E_b$, $\tilde{\gamma} = \gamma/\gamma_b$, where L_0 is a characteristic macroscopic length used to get a non-dimensional space variable, u_0 is a characteristic displacement E_b and γ_b are constant first and second gradient elastic moduli which we chose to be that of compact bone. With these notations, the dimensionless form of the bulk equation (14), after integrating it both in the regions $X \in [L/2, L]$ and $X \in [0, L/2]$ and using the two appropriate boundary conditions to determine the integration constants gives on both sides of the discontinuity

$$\tilde{E}\tilde{y} - \left(\tilde{\mathbb{E}}\tilde{y}'\right)' = \tilde{F}_0^{ext} \tag{17}$$

where, with a slight abuse of notation the apex now indicates derivation with respect to the dimensionless variable $\tilde{x}$, we set $\tilde{y} := \tilde{u}'$, $\tilde{F}_0^{ext} = f^{ext} N L_0/(E_b u_0)$ and moreover

$$\tilde{E} := \frac{E}{E_b} = \left(\tilde{E}_b \left(\frac{\rho_b^*}{\rho_{\max}}\right)^\beta + \tilde{E}_m \left(\frac{\rho_m^*}{\rho_{\max}}\right)^\beta\right), \qquad \tilde{\mathbb{E}} := \frac{\gamma N}{E_b L_0^2} = \left(\tilde{\mathbb{E}}_b \left(\frac{\rho_b^*}{\rho_{\max}}\right)^\alpha + \tilde{\mathbb{E}}_m \left(\frac{\rho_m^*}{\rho_{\max}}\right)^\alpha\right) \tag{18}$$

with

$$\tilde{E}_b = \frac{E_b}{E_b} = 1, \qquad \tilde{E}_m = \frac{E_m}{E_b}, \qquad \tilde{\mathbb{E}}_b = \frac{\gamma_b N}{E_b L_0^2} =: N\left(\frac{l_b}{L_0}\right)^2, \qquad \tilde{\mathbb{E}}_m = \frac{\gamma_m N}{E_b L_0^2} =: N\left(\frac{l_m}{L_0}\right)^2 \tag{19}$$

The introduced quantities l_b and l_m are second gradient characteristic lengths related to the micro-structure of natural bone and bio-material respectively (see e.g. [76,77] for some explanations of the meaning of second gradient characteristic lengths). Indeed, the physical meaning of these second gradient characteristic lengths is not immediate, but it is known to be related to the stiffness of the microscopic heterogeneities of the considered continua: we refer to [78] for an extended treatment of microscopically heterogeneous materials by means of generalized theories. The remaining boundary conditions which have not been used to determine the integration constants and which do not involve only the zero-th order derivatives of displacement are written in their dimensionless form as

$$\tilde{y} = 0 \quad \text{in} \quad \tilde{x} = 0$$
$$\left[|\tilde{y}|\right] = 0, \qquad \left[|\tilde{\mathbb{E}}\tilde{y}'|\right] = 0 \quad \text{in} \quad \tilde{x} = \frac{1}{2}\frac{L}{L_0}$$
$$\tilde{\mathbb{E}}\tilde{y}' = 0 \quad \text{in} \quad \tilde{x} = \frac{L}{L_0} \tag{20}$$

We explicitly remark that Eq. (17) is valid on both sides of the discontinuity surface: we actually have two unknown displacements u^+ and u^-. Nevertheless, due to the used boundary conditions the external force f^{ext} considered in the bulk equation is always the same on both sides.

We also want to find a dimensionless form of the biological evolution equations: dividing Eqs. (5) by $\rho_{\max}$, introducing the dimensionless time $\tilde{t} = t/t_0$ and considering the constitutive assumptions (7), their dimensionless form reads

$$\frac{\partial}{\partial \tilde{t}}\left(\frac{\rho_b^*}{\rho_{\max}}\right) = H(\varphi^*)\tilde{A}_b(\tilde{S}^*), \qquad \frac{\partial}{\partial \tilde{t}}\left(\frac{\rho_m^*}{\rho_{\max}}\right) = H(\varphi^*)\tilde{A}_m(\tilde{S}^*) \tag{21}$$

In these equations we set

$$H = k\varphi^*(1 - \varphi^*), \qquad \tilde{A}_b(\tilde{S}^*) = \begin{cases} \tilde{s}_b\tilde{S}^* & \text{for } \tilde{S}^* > 0, \\ \tilde{r}_b\tilde{S}^* & \text{for } \tilde{S}^* < 0, \end{cases} \qquad \tilde{A}_m(S) = \begin{cases} 0 & \text{for } \tilde{S}^* > 0 \\ \tilde{r}_m\tilde{S}^* & \text{for } \tilde{S}^* < 0 \end{cases} \tag{22}$$

where φ^* is still given by Eq. (8) and moreover

$$\tilde{s}_b = \frac{U_0 L_0 t_0}{\rho_{\max}} s_b, \qquad \tilde{r}_b = \frac{U_0 L_0 t_0}{\rho_{\max}} r_b, \qquad \tilde{r}_m = \frac{U_0 L_0 t_0}{\rho_{\max}} r_m, \quad U_0 = \frac{E_b}{N}\left(\frac{u_0}{L_0}\right)^2 \tag{23}$$

Finally, the dimensionless Lagrangian stimulus $\tilde{S}^*$ appearing in (22) is

$$\tilde{S}^*(\tilde{x},\tilde{t}) = \frac{S^*}{U_0 L_0} = \left(\int_0^{L/L_0} \tilde{U}^*(\tilde{x}_0,\tilde{t}) d^*(\tilde{x}_0,t) \exp\left(-\tilde{D}\left\| \tilde{x} - \tilde{x}_0 + \frac{u_0}{L_0}\big(\tilde{u}(L_0\tilde{x}) - \tilde{u}(L_0\tilde{x}_0)\big)\right\|\right) d\tilde{x}_0 \right) - \tilde{S}_0^*(\tilde{x},\tilde{t}) \tag{24}$$

where

$$\tilde{U}^* = \frac{U^*}{U_0} = \frac{1}{2}\tilde{E}\tilde{y}^2 + \frac{1}{2}\tilde{\mathbb{E}}(\tilde{y}')^2 \tag{25}$$

and where we introduced the new dimensionless quantities $\tilde{D} = DL_0$, $\tilde{x}_0 = X_0/L_0$ and $\tilde{S}_0^* = S_0^*/(U_0 L_0)$. Note that, since in linear elasticity the quantity u_0/L_0 is often very small, the third term inside the norm can be neglected in most of practical applications. Summarizing, we can say that the problem which will be treated in the following numerical simulations will consist of the following steps:

(i) Fix (for any t) the constitutive values of the parameters of the proposed model (see e.g. Tables 1 and 2);
(ii) Fix initial values for the mass densities $\rho_b^*/\rho_{\max}$ and $\rho_m^*/\rho_{\max}$ (the initial values of $\tilde{E}$ and $\tilde{\mathbb{E}}$ are fixed as well in virtue of Eqs. (18));
(iii) Solve the differential equations (17) equipped with the boundary conditions (20) to determine $\tilde{y}$;
(iv) Calculate the strain energy density by means of Eq. (25) and the fraction of osteocytes by using Eq. (9)$_2$;
(v) Calculate the biological stimulus by means of Eq. (24);
(vi) Calculate the mass densities $\rho_b^*/\rho_{\max}$ and $\rho_m^*/\rho_{\max}$ at the subsequent time step by means of Eqs. (21);
(vii) Come back to point (iii) and repeat up to convergence.

We explicitly remark that the introduced continuum mixture model allows for the description of changes in the distribution of the two-solid phases present in reconstructed bone grafts. Indeed, the bio-resorbable material can be resorbed and replaced by natural bone tissue giving birth to phenomena which are similar to phase transitions of the type described e.g. in [79].

4. Numerical simulations

We start by choosing the values of the constitutive parameters as shown in Tables 1 and 2.

Table 1
Values of the parameters used in numerical simulations.

$\rho_b/\rho_{\max}$ at $t=0$	$\rho_m/\rho_{\max}$ at $t=0$	k	θ	η	$\tilde{s}_b$	$\tilde{r}_b$	$\tilde{r}_m$
0.5	0.5	4	1	1	10	10	15

Table 2
Values of the parameters used in numerical simulations.

$\tilde{F}_0^{ext}$	$\tilde{E}_b$	$\tilde{E}_m$	N	β	α	$\tilde{D}$	$\tilde{S}_0^*$
2.5	1	1	1	1.9	6	10	0.1

The second gradient parameters are chosen such that $\tilde{\mathbb{E}}_b = \tilde{\mathbb{E}}_m$ and different values are tested in order to evidence some scale effects related to second gradient. In this paper we limit ourselves to test a set of some values of $\tilde{\mathbb{E}}_b = \tilde{\mathbb{E}}_m$ in the interval $[0.55, 1]$ (region included between the dashed lines in Fig. 1) in order to show some preliminary results indicating that our theory is able to encompass that kind of scale effects which are experimentally observed in bone specimens smaller than 1 mm as explained e.g. in [38]. We will also show that the considered values of the second gradient parameters cannot be considered negligible as they macroscopically affect the phenomenon of reconstructed bone remodelling with respect to the classical first gradient case. In a forthcoming paper we will present a systematic parametric study showing analogous results for a wider range of values of the second gradient parameters and we will show how the results obtained by means of the classical Cauchy continuum theory can be obtained as a limit case of the used second gradient theory by letting $\tilde{\mathbb{E}}_b$ and $\tilde{\mathbb{E}}_m$ go to zero.

We fix the second gradient characteristic length to be of the order of the size of osteons, i.e. $l_b = l_m = 10^{-4}$ m and we suitably choose the adimensionalisation length L_0 to be proportional to the length L of the specimen (we choose here $L = 7.5L_0$). In this way, in virtue of the constitutive equations (19) and for any chosen value of the non-dimensional second
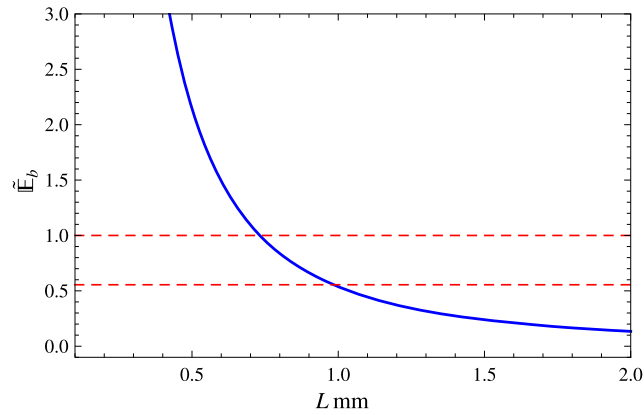
Fig. 1. Dependence of the second gradient elasticity parameter on the length of the considered specimen (values of the second gradient parameters tested here in the interval delimited by the two dashed lines).

gradient parameters, we are able to come back to the length L of the specimen. We show in Fig. 1 the obtained dependence of the second gradient parameter $\tilde{\mathbb{E}}_b$ on the length of the specimen (an identical behavior is envisaged for $\tilde{\mathbb{E}}_m$). We can notice from Fig. 1 that the second gradient parameter becomes more and more important for decreasing sizes of the specimen. This is in agreement with experimental evidences (of the type presented e.g. in [38]) which show this type of scale effects for small specimens. It is then clear that for specimens which are small enough to have their macroscopic deformation considerably influenced by the presence of the underlying micro-structure, the use of second gradient or otherwise generalized theories is mandatory (see also [51,38,52,50]). We also show in the following pictures the effect that second gradient has on the final percentages of replacement by comparison with the equilibrium configuration obtained via a Cauchy continuum theory. To do so, we start by showing in Fig. 2 the initial distribution of dimensionless densities which are used in all first and second gradient numerical simulations. In Fig. 2 and in the following we will show together two ways of displaying the distribution of the mass densities at a given time. In particular, the first picture on the left side shows a quantitative distribution of the (non-dimensional) densities of the two constituents in the considered specimen, while the second picture on the right shows the corresponding qualitative distribution of the bio-material (blue) and natural bone (red) separately (first two smaller upper bars) and when considered together in the mixture (bigger lower bar). The intensity of colours in the qualitative picture is directly proportional to the value of mass density, following a criterion which is analogous to the one used in Litmus paper (small paper used to measure pH of solutions). The black colour indicates absence of the considered constituent (mass density $= 0$).

As already shown in Table 2, we apply an external dimensionless force $\tilde{F}_0^{ext} = 2.5$ and, for any chosen value of the dimensionless second gradient parameter, we look for the equilibrium configuration of the specimen by following the steps (i)–(vii) detailed in the previous section. We start by showing in Fig. 3 the equilibrium configuration obtained when $\tilde{\mathbb{E}}_b = \tilde{\mathbb{E}}_m = 0$, which is the limit case of classical Cauchy continuum theory.

By comparison of Figs. 2 and 3 we can notice that creation of new bone tissue occurs in the region originally occupied by natural bone tissue (left half of the specimen) as a result of the application of the external mechanical excitation. As far as the region originally occupied by artificial bio-resorbable material (right half of the specimen) is concerned, we can notice how the application of the external mechanical load triggers the resorption of the bio-material which is subsequently replaced by natural bone tissue. We can see in Fig. 3 that, at the end of the process of remodelling, an extended region of a natural-bone/artificial-material composite still exists even far from the initial discontinuity surface. The fact that the artificial material is not completely resorbed can be explained with the following mechanisms taking place during the remodelling process: (i) The signal sent by the osteocytes (which are initially located only in the left half of the specimen) reaches the actor cells which are located in the artificial material and which are closer to the discontinuity surface. This signal is intense enough that no resorption of bio-material takes place and natural bone tissue starts being created. (ii) This process of generation of new natural tissue close to the interface is so rapid that the available porosity is quickly filled and no more space is available for the actor cells to deposit and continue synthesizing more natural tissue. (iii) In regions of the artificial material which are far from the interface, the biological stimulus reaching the actor cells is lower than the chosen threshold value, so that resorption of the artificial bio-material starts taking place. At the same time, since new natural tissue is forming close to the interface and starts propagating in the bio-material region (points (i) and (ii)), a more and more intense stimulus is perceived by actors cells which starts synthesizing natural bone tissue once that the intensity of the stimulus overcomes the threshold value (i.e. S^* becomes positive). (iv) A more pronounced resorption occurs far from the interface since the osteoclasts have more time to resorb the artificial material before that the intensity of the stimulus overcomes the threshold value and that natural bone tissue synthesis occurs.

A more accurate study of the actual thickness of this natural-bone/bio-material composite inclusion should be carried out by refining the mesh of the adopted numerical scheme, above all close to the discontinuity surface. This will be the object of further work.

Initial distribution of tissue and bio-material
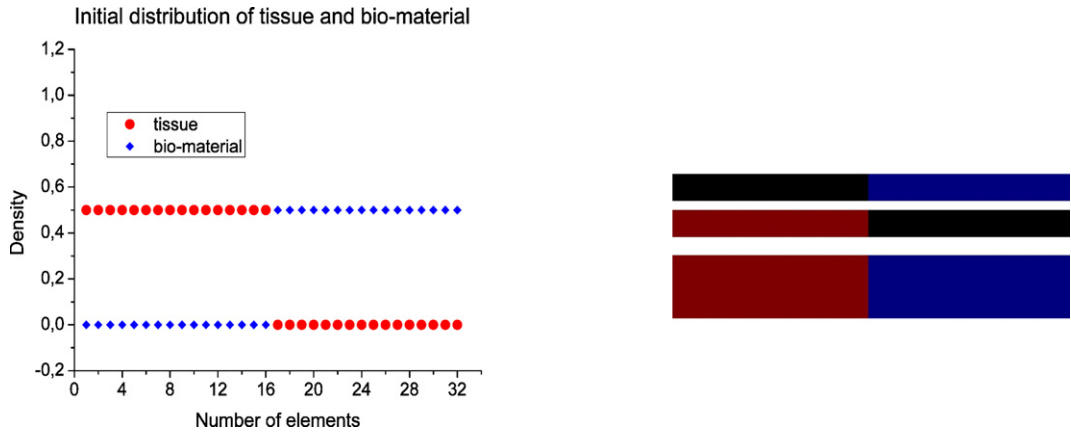
Fig. 2. Initial distribution of natural bone and artificial bio-material mass densities in the considered specimen.
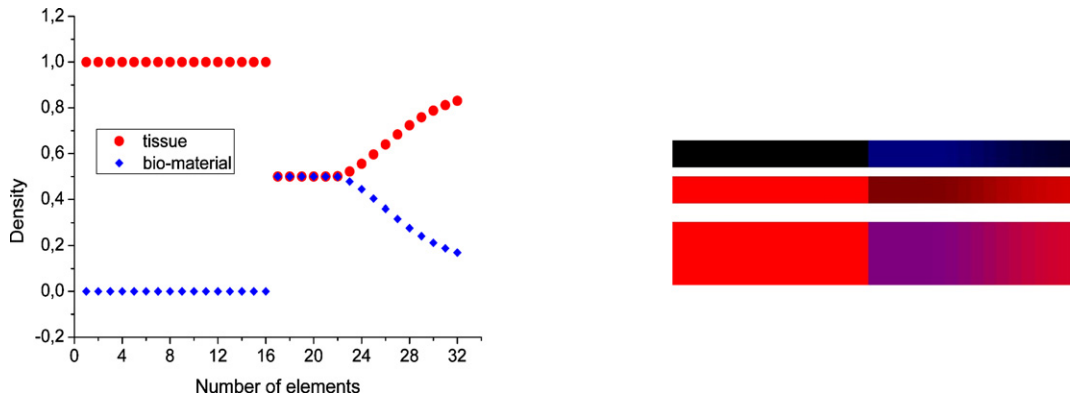
Fig. 3. Final distribution of natural bone and artificial bio-material mass densities in classical Cauchy continuum case (any length *L*).
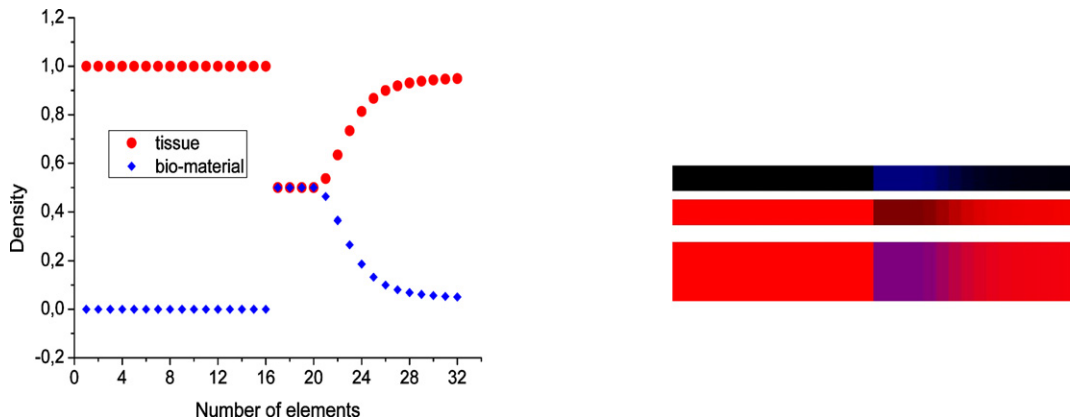
Fig. 4. Final distribution of natural bone and artificial bio-material mass densities in the case $\tilde{\mathbb{E}}_b = \tilde{\mathbb{E}}_m = 1$ ($L \approx 0.75$ mm).

As in Cauchy continuum theory no characteristic lengths accounting for micro-structure are present, one gets the same picture at equilibrium for any length of the considered specimen. Indeed, if this is reasonable for big specimens of the order of ten millimeters or more, this is not true for smaller specimens, as it has been widely proven by experiments. In fact, when sufficiently small specimens are considered, the osteons which constitute the first-level bone micro-structure start playing an important role on the deformation patterns of the continuum so giving a non-negligible contribution to its overall deformation.

In Figs. 4–7 we show the different equilibrium configurations attained when decreasing the values of the non-dimensional second gradient parameters from 1 to 0.65. We can observe visible differences in the equilibrium configuration of the remodelling process also for small variations of the second gradient parameters. These differences are related to the
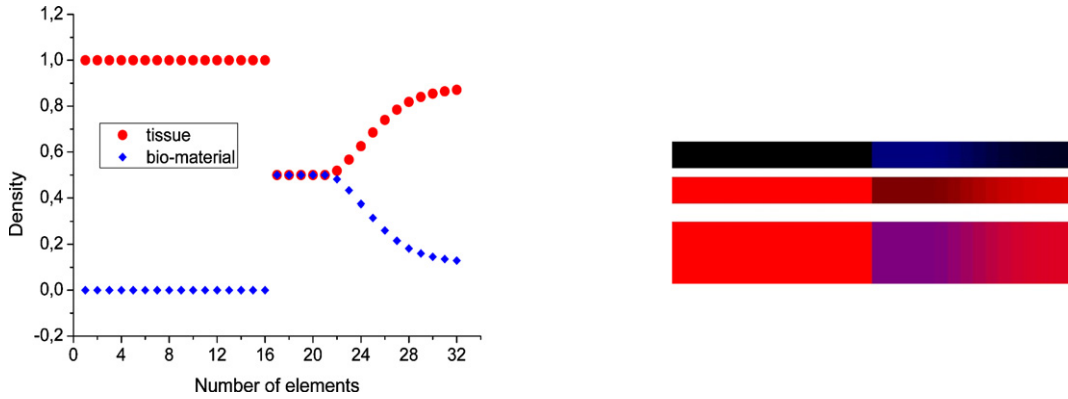
Fig. 5. Final distribution of natural bone and artificial bio-material mass densities in the case $\tilde{\mathbb{E}}_b = \tilde{\mathbb{E}}_m = 0.8$ ($L \approx 0.84$ mm).
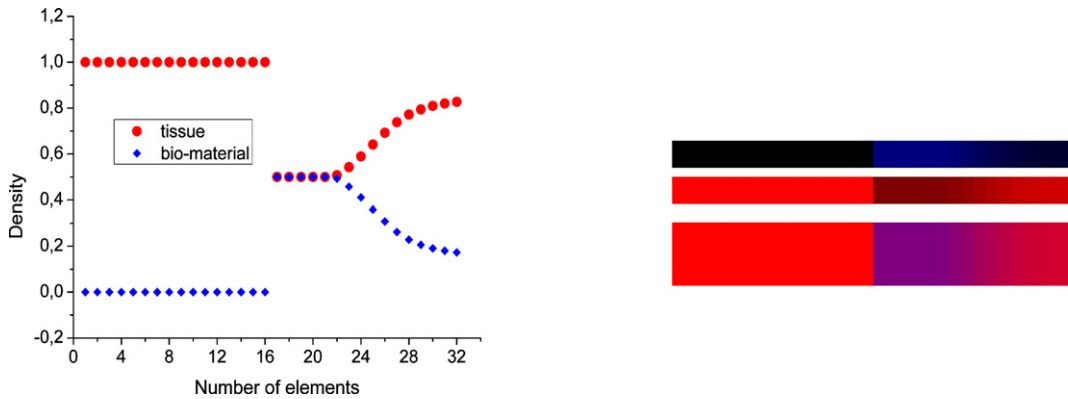
Fig. 6. Final distribution of natural bone and artificial bio-material mass densities in the case $\tilde{\mathbb{E}}_b = \tilde{\mathbb{E}}_m = 0.7$ ($L \approx 0.9$ mm).
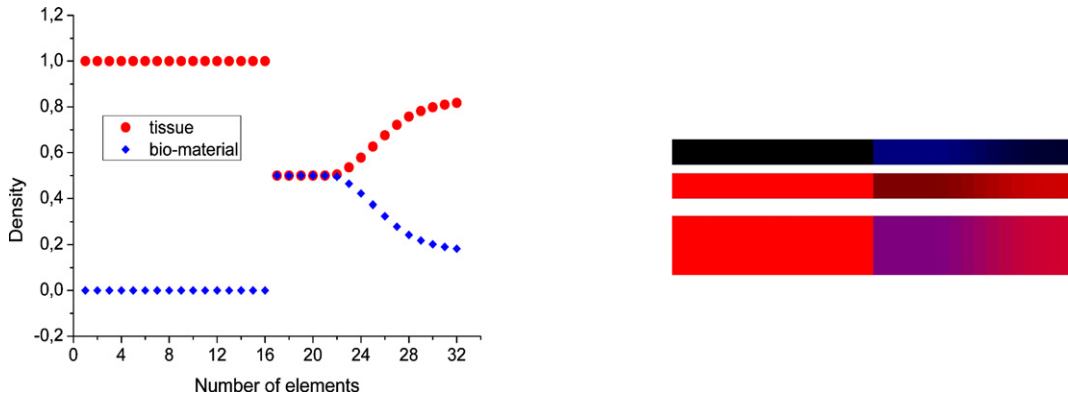
Fig. 7. Final distribution of natural bone and artificial bio-material mass densities in the case $\tilde{\mathbb{E}}_b = \tilde{\mathbb{E}}_m = 0.65$ ($L \approx 0.93$ mm).

fact that a second gradient theory accounts for the effect of micro-structure on the overall deformation of the considered material. In particular, the fact of accounting for the presence of a micro-structure in bone and bio-material considerably changes the value of the calculated strain energy which thus results in a considerable variation of the biological stimulus and hence, finally, of the overall remodelling process.

The numerical simulations presented in Figs. 4–7 show that an increase in the second gradient parameter results in a more pronounced substitution of artificial bio-material with natural bone tissue. In particular, in Fig. 4 (corresponding to the case $\tilde{\mathbb{E}}_b = \tilde{\mathbb{E}}_m = 1$) the maximum percentage of replacement of bio-material with natural bone tissue is observed. This means that the calculated value of the SED resulting from the application of the external load is macroscopically affected by the presence of the second gradient term (see Eq. (25)) and so is the biological stimulus. By comparison of Figs. 4 and 7 we can notice that the thickness of the residual natural-bone/artificial-material composite is sensibly different in the two cases (up to 50%).
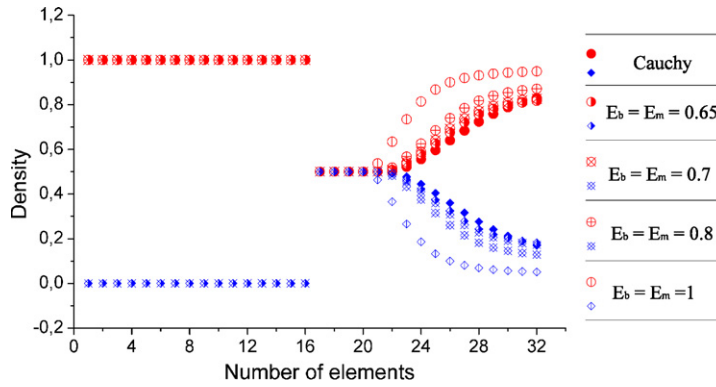
Fig. 8. Final distribution of natural bone and artificial bio-material mass densities for different values of the second gradient parameters.

We can then conclude that the fact of using a classical Cauchy theory to describe deformation of the considered system would lead to under/over-estimations of the calculated SED, so resulting in macroscopic errors in the estimation of the equilibrium configuration attained at the end of the remodelling process. It is then clear that, above all when considering small specimens (or equivalently external loads which excite the heterogeneous micro-structure), the use of generalized theories for the study of deformation of reconstructed bones becomes mandatory and it therefore deserves to be investigated with more refined numerical investigations.

In order to perform a direct comparison of the results presented in Figs. 4–7, we present them grouped in a unique picture in Fig. 8.

5. Conclusions

In this article we present the theoretical framework which is needed to account for an internal length (characteristic of the micro-structure of reconstructed bone) and for its effect on reconstructed bone remodelling by means of the use of a second gradient theory. A one-dimensional example is addressed in which natural bone and artificial bio-material are initially in contact through a material discontinuity surface. The presented numerical simulations show that the effect of micro-structure on the overall process of remodelling of both natural bone and bio-material may be non-negligible. These results are encouraging and in agreement with the experimental observation of size effects in bone which are directly related to the hierarchical micro-structure of this complex material (see e.g. [38,69,44,80,47]). In a subsequent paper we will present a systematic parametric study in which the effect of all the introduced biological and mechanical parameters on the reconstructed bone remodelling process will be carefully investigated. Due to the complexity of the phenomena to be described, the biological and mechanical parameters associated to the introduced continuum model are numerous and their single effect on reconstructed bone remodelling therefore needs to be isolated and evaluated. Wider ranges of values of the second gradient parameters will be tested in future work and the limit case of classical first gradient theory will be recovered by letting the second gradient parameters tend to zero. The study of the influence of second gradient on more complicated geometries and loading conditions is also interesting and so deserves attention in future investigations.

Appendix A. Variational deduction of the equilibrium equation and of the associated duality conditions

Let $[0, T]$ be a time interval and B_L the Lagrangian configuration of the system, then the action functional of the considered second gradient continuum is defined as

$$\mathcal{A} = \int_0^T \int_{B_L} U^*(\boldsymbol{\varepsilon}, \nabla \boldsymbol{\varepsilon}) \tag{A.1}$$

where we recall that U^* is the Lagrangian strain energy density per unit volume and $\boldsymbol{\varepsilon} = (\mathbf{F}^T \cdot \mathbf{F} - \mathbf{I})/2$ denotes the Green–Lagrange deformation tensor. We want to calculate a stationary point of the action functional by computing its first variation $\delta \mathcal{A}$ and imposing it to be vanishing. This will allow for determining the equilibrium equation of the system and the associated duality conditions which must be respected at any surface of discontinuity of the considered medium. Assuming that the considered kinematical field is suitably regular we can write the first variation of the action functional as

$$\delta \mathcal{A} = \int_0^T \int_{B_L} \left(\frac{\partial U^*}{\partial \boldsymbol{\varepsilon}} \mid \delta \boldsymbol{\varepsilon} + \frac{\partial U^*}{\partial \nabla \boldsymbol{\varepsilon}} \mid \delta \nabla \boldsymbol{\varepsilon} \right) \tag{A.2}$$

where the symbol | stands for the usual scalar product between two tensor fields of the same order[2] and, for any Lagrangian field a, the symbol δa stands for its variation. Setting $\mathbf{A} = \partial U^*/\partial \boldsymbol{\varepsilon}$ and $\mathbf{B} = \partial U^*/\partial \nabla \boldsymbol{\varepsilon}$ (with components A_{ij} and B_{ijk} respectively) using the symmetry of the second order tensor $\mathbf{A}$, and the symmetry of the third order tensor $\mathbf{B}$ with respect to its first two indices it can be checked that

$$\mathbf{A} \,|\, \delta \boldsymbol{\varepsilon} = \mathbf{A} \,|\, \big(\mathbf{F}^T \cdot \delta \mathbf{F}\big), \qquad \mathbf{B} \,|\, \delta \nabla \boldsymbol{\varepsilon} = \mathbf{B} \,|\, \nabla \big(\delta \mathbf{F}^T \cdot \mathbf{F}\big)$$

Integrating by parts a suitable number of times and recalling that $\mathbf{F} = \nabla \boldsymbol{\chi}$, Eq. (A.2) can be written in components as

$$\delta \mathcal{A} = -\int\limits_0^T \int\limits_{B_L} \big[(A_{ij} - B_{ijp,p})\mathbf{F}_{ki}\big]_{,j} \delta \boldsymbol{\chi}_k + \int\limits_0^T \int\limits_{B_L} \big[(A_{ij} - B_{ijp,p})\mathbf{F}_{ki}\delta \boldsymbol{\chi}_k\big]_{,j} + \int\limits_0^T \int\limits_{B_L} [B_{ijp}\mathbf{F}_{kj}\delta \mathbf{F}_{ki}]_{,p}$$

Using the divergence theorem and considering test functions which have compact support K included in B_L having non-empty intersection Σ_K with the discontinuity surface Σ, the previous equation implies

$$\delta \mathcal{A} = -\int\limits_0^T \int\limits_K \big[(A_{ij} - B_{ijp,p})\mathbf{F}_{ki}\big]_{,j} \delta \boldsymbol{\chi}_k + \int\limits_0^T \int\limits_{\Sigma_K} \big[\big|(A_{ij} - B_{ijp,p})\mathbf{F}_{ki}n_j\delta \boldsymbol{\chi}_k\big|\big]$$

$$+ \int\limits_0^T \int\limits_{\Sigma_K} \big[\big|B_{ijp}\mathbf{F}_{kj}\delta \boldsymbol{\chi}_{k,i}n_p\big|\big] \tag{A.3}$$

where n_j denote the components of the unit normal vector $\mathbf{n}$ to Σ_K. The last term of the sum appearing in Eq. (A.3) involves the quantity $\nabla \delta \boldsymbol{\chi}$ and can still be manipulated. To do so, it is worth decomposing this tensor by projecting it in the normal and tangent direction to the surface Σ_K as[3]

$$\nabla \delta \boldsymbol{\chi} = \nabla \delta \boldsymbol{\chi} \cdot (\mathbf{n} \otimes \mathbf{n}) + \nabla \delta \boldsymbol{\chi} \cdot (\mathbf{I} - \mathbf{n} \otimes \mathbf{n}) =: (\delta \boldsymbol{\chi})_n \otimes \mathbf{n} + \nabla^{\Sigma} \delta \boldsymbol{\chi}$$

With this decomposition, it can be checked that Eq. (A.3) implies

$$\delta \mathcal{A} = -\int\limits_0^T \int\limits_K \big[(A_{ij} - B_{ijp,p})\mathbf{F}_{ki}\big]_{,j} \delta \boldsymbol{\chi}_k + \int\limits_0^T \int\limits_{\Sigma_K} \big[\big|(A_{ij} - B_{ijp,p})\mathbf{F}_{ki}n_j\delta \boldsymbol{\chi}_k\big|\big]$$

$$+ \int\limits_0^T \int\limits_{\Sigma_K} \big[\big|B_{ijp}\mathbf{F}_{kj}\big((\delta \boldsymbol{\chi})_n\big)_k n_i n_p\big|\big] + \int\limits_0^T \int\limits_{\Sigma_K} \big[\big|B_{\alpha jp}\mathbf{F}_{kj}\delta \boldsymbol{\chi}_{k,\alpha}n_p\big|\big]$$

Integrating by parts the last term in the previous equation and using the surface divergence theorem we can finally write

$$\delta \mathcal{A} = -\int\limits_0^T \int\limits_K \big[(A_{ij} - B_{ijp,p})\mathbf{F}_{ki}\big]_{,j} \delta \boldsymbol{\chi}_k + \int\limits_0^T \int\limits_{\Sigma_K} \big[\big|(A_{ij} - B_{ijp,p})\mathbf{F}_{ki}n_j\delta \boldsymbol{\chi}_k\big|\big] - \int\limits_0^T \int\limits_{\Sigma_K} \big[\big|(B_{\alpha jp}\mathbf{F}_{kj}n_p)_{,\alpha}\delta \boldsymbol{\chi}_k\big|\big]$$

$$+ \int\limits_0^T \int\limits_{\Sigma_K} \big[\big|B_{ijp}\mathbf{F}_{kj}\big((\delta \boldsymbol{\chi})_n\big)_k n_i n_p\big|\big] + \sum_{i=1}^N \int\limits_0^T \int\limits_{\mathcal{E}_{\Sigma}} \big[\big|B_{\alpha jp}\mathbf{F}_{kj}n_p\delta \boldsymbol{\chi}_k \nu_{\alpha}\big|\big]$$

where $\mathcal{E}_i$, $i = 1, \dots, N$ are the edges of the surface Σ_K (if any) and ν_{α} are the components of the normal $\boldsymbol{\nu}$ to the border of Σ_k (if the edge is regarded as the border of a surface then $\boldsymbol{\nu}$ is the normal vector to the considered edge which is tangent to the surface). In this last formula, with a slight abuse of notation we indicate with the same notation the jump across a surface and the jump across a line. Staring from this last expression for $\delta \mathcal{A}$, recalling that $\mathbf{B}$ is symmetric with respect to its first two indices, that $\delta \boldsymbol{\chi} = \delta \mathbf{u}$ and assuming that the test functions are arbitrary in the bulk but not necessarily on the discontinuity surface, it can be checked that the condition $\delta \mathcal{A} = 0$ implies the bulk equation (1) and the duality conditions (2).

---

[2] Let for example $\mathbf{A}$ and $\mathbf{B}$ be two third order tensors of components A_{ijk} and B_{ijk} respectively. Their scalar product is defined as $\mathbf{A} \,|\, \mathbf{B} = A_{ijk}B_{ijk}$, where the Einstein summation convention over repeated indexes is used.

[3] Here and in the sequel, given any field a the symbol $(a)_n := \nabla a \cdot \mathbf{n}$ stands for the normal derivative of the field a, while the symbol $\nabla^{\Sigma} a$ stands for its surface gradient. To write in components the gradient on the surface we use Greek letters. In particular we set $(\nabla^{\Sigma} a)_{\alpha} =: a_{,\alpha}$.

Appendix B. Deduction of the one-dimensional equilibrium equation

We show here how the one-dimensional equilibrium equation (14) is deduced starting from its 3D version (1). It can be easily checked that assuming the hypothesis of small displacements (which implies neglecting quadratic terms) considering expressions (10) for **F** and $\boldsymbol{\varepsilon}$ respectively and expression (11) for the strain energy density U^* implies that the only non-vanishing component of Eq. (14) is

$$\left((\lambda + 2\mu)u'\right)' - \left(\gamma u''\right)'' = 0 \tag{B.1}$$

Recalling now that the Lamé parameters are given in terms of the Young modulus and of the Poisson coefficient by means of the relations

$$\lambda = \frac{E\nu}{(1+\nu)(1-2\nu)}, \qquad \mu = \frac{E}{2(1+\nu)} \tag{B.2}$$

it is easy to check that the one-dimensional equilibrium equation (B.1) finally implies Eq. (14).

With analogous reasoning it is possible to show that the one-dimensional form of the duality conditions (2) implies

$$\left[\left|\left((\lambda + 2\mu)u' - \left(\gamma u''\right)'\right)\delta u\right|\right] = 0, \qquad \left[\left|\gamma u''(\delta u)_n\right|\right] = 0 \tag{B.3}$$

Recalling Eqs. (B.2), considering that in the simple one-dimensional case considered here $(\delta u)_n = \delta u'$ it is immediate to check that the aforementioned duality conditions are compatible with the boundary conditions (15) used in the proposed numerical problem.

References

[1] D.R. Carter, M.C.H. Van der Meulen, G.S. Beaupré, Mechanical factors in bone growth and development, Bone 18 (1996) S5–S10.
[2] R. Casanova, D. Moukoko, M. Pithioux, C. Pailler-Mattéi, H. Zahouani, P. Chabrand, Temporal evolution of skeletal regenerated tissue: What can mechanical investigation add to biological?, Med. Biol. Eng. Comput. 48 (2010) 811–819.
[3] R. Huiskes, R. Ruimerman, G.H. van Lenthe, J.D. Janssen, Effects of mechanical forces on maintenance and adaptation of form in trabecular bone, Nature 405 (2000) 704–706.
[4] A. Madeo, T. Lekszycki, F. dell'Isola, A continuum model for the bio-mechanical interactions between living tissue and bio-resorbable graft after bone reconstructive surgery, C. R., Méc. 339 (2011) 625–640.
[5] T. Lekszycki, Optimality conditions in modeling of bone adaptation phenomenon, J. Theoret. Appl. Mech. 37 (3) (1999) 607–624.
[6] T. Lekszycki, Modeling of bone adaptation based on an optimal response hypothesis, Meccanica 37 (2002) 343–354.
[7] T. Lekszycki, Functional adaptation of bone as an optimal control problem, J. Theoret. Appl. Mech. 43 (3) (2005) 120–140.
[8] J. Wolff, Das Gesetz der Transformation der Knochen, Hirschwald Verlag, Berlin, 1892.
[9] J. Wolff, The Law of Bone Remodelling, Springer-Verlag, Berlin, 1986.
[10] M. Pawlikowski, M. Klasztorny, K. Skalski, Studies on constitutive equation that models bone tissue, Acta Bioeng. Biomech. 10 (4) (2008) 39–47.
[11] R. Ruimerman, P. Hilbers, B. van Rietbergen, R. Huiskes, A theoretical framework for strain-related trabecular bone maintenance and adaptation, J. Biomech. 38 (2005) 931–941.
[12] D.H. Hegedus, S.C. Cowin, Bone remodeling II: Small strain adaptive elasticity, J. Elast. 6 (1976) 337–352.
[13] U. Andreaus, M. Colloca, D. Iacoviello, M. Pignataro, Optimal-tuning PID control of adaptive materials for structural efficiency, Struct. Multidiscipl. Optim. 43 (2011) 43–59.
[14] U. Andreaus, M. Colloca, Prediction of micromotion initiation of an implanted femur under physiological loads and constraints using the finite element method, Proc. Inst. Mech. Eng., H J. Eng. Med. 223 (2009) 589–605.
[15] P.J. Prendergast, D. Taylor, Prediction of bone adaptation using damage accumulation, J. Biomech. 27 (1994) 1067–1076.
[16] M. Doblaré, J.M. García, Anisotropic bone remodelling model based on a continuum damage-repair theory, J. Biomech. 35 (2002) 1–17.
[17] T. Goto, T. Kojima, T. Iijima, S. Yokokura, H. Kawano, A. Yamamoto, K. Matsuda, Resorption of synthetic porous hydroxyapatite and replacement newly formed bone, J. Orthop. Sci. 6 (2001) 444–447.
[18] J.F. Mano, R.A. Sousa, L.F. Boesel, N.M. Neves Rui, L. Reis, Bioinert, biodegradable and injectable polymeric matrix composites for hard tissue replacement: State of the art and recent developments, Compos. Sci. Technol. 64 (2004) 789–817.
[19] A.F. Schilling, W. Linhart, S. Filke, M. Gebauer, T. Schinke, J.M. Rueger, M. Amling, Resorbability of bone substitute biomaterials by human osteoclasts, Biomaterials 25 (2004) 3963–3972.
[20] V.I. Sikavitsas, J.S. Temenoff, A.G. Mokos, Review: Biomaterials and bone mechanotransduction, Biomaterials 22 (2001) 2581–2593.
[21] A.S. Greenwald, S.D. Boden, V.M. Goldberg, Y.K. Cato, T. Laurencin, R.N. Rosier, Bone graft substitutes: Facts, fictions & applications, in: 68th Annual Meeting American Academy of Orthopaedic Surgeons, San Francisco, California, February 28–March 4, 2001.
[22] K.A. Hing, Bioceramic bone graft substitutes: Influence of porosity and chemistry, Int. J. Appl. Ceram. Technol. 2 (3) (2005) 184–199.
[23] H.-M. Kim, Ceramic bioactivity and related biomimetic strategy, Curr. Opin. Solid State Mater. Sci. 7 (2003) 289–299.
[24] R. Kraus, J.-P. Stahl, R. Schnettler, Treatment strategies in thoracolumbar vertebral fractures: Are there indications for biomaterials?, European J. Trauma (2007) 253–257.
[25] J.C. Park, D. Wook, H. Suh, A bone replaceable artificial bone substitute: Morphological and physiochemical characterizations, Yonsei Med. J. 41 (4) (2000) 468–476.
[26] M. Pawlikowski, K. Skalski, M. Haraburda, Process of hip joint prosthesis design including bone remodeling phenomenon, Comput. Struct. 81 (8–11) (2003) 887–893.
[27] S. Pietruszczak, D. Inglis, G.N. Pande, Modelling of bone–implant interaction, Comput. Methods Biomech. Biomed. Eng. 2 (1998) 289–298.
[28] S. Piszczatowski, K. Skalski, W. Swieszkowski, Load transfer between elastic hip implant and viscoelastic bone, Comput. Methods Biomech. Biomed. Eng. 2 (1998) 123–130.
[29] Y. Ramaswamy, D.R. Haynes, G. Berger, R. Gildenhaar, H. Lucas, Bioceramics composition modulate resorption of human osteoclasts, J. Mater. Sci., Mater. Med. 16 (2005) 1199–1205.
[30] J.A. Sanz-Herrera, A.R. Boccaccini, Modelling bioactivity and degradation of bioactive glass based tissue engineering scaffolds, Int. J. Solids Struct. 48 (2010) 257–268.

[31] J.A. Sanz-Herrera, J.M. García-Aznar, M. Doblaré, Micro–macro numerical modelling of bone regeneration in tissue engineering, Comput. Methods Appl. Mech. Eng. 197 (2008) 3092–3107.

[32] E. Kuhl, G.A. Holzapfel, A continuum model for remodeling in living structures, J. Mater. Sci. 42 (21) (2007) 8811–8823.

[33] S.C. Cowin, Bone poroelasticity, J. Biomech. 32 (1999) 217–238.

[34] S.C. Cowin, D.H. Hegedus, Bone remodeling I: Theory of adaptive elasticity, J. Elast. 6 (1976) 313–326.

[35] K. Garikipati, E.M. Arruda, K. Grosh, H. Narayanan, S. Calve, A continuum treatment of growth in biological tissue: The coupling of mass transport and mechanics, J. Mech. Phys. Solids 52 (2004) 1595–1625.

[36] T. Adachi, Y. Osako, M. Tanaka, M. Hojo, S.J. Hollister, Framework for optimal design of porous scaffold microstructure by computational simulation of bone regeneration, Biomaterials 27 (21) (2006) 3964–3972.

[37] Y. Chen, S. Zhou, Q. Li, Microstructure design of biodegradable scaffold and its effect on tissue regeneration, Biomaterials 32 (22) (2011) 5003–5014.

[38] P.M. Buechner, R.S. Lakes, Size effects in the elasticity and viscoelasticity of bone, Biomech. Model. Mechanobiol. 1 (2003) 295–301.

[39] T.P. Harrigan, M. Jasty, R.W. Mann, W.H. Harris, Limitations of the continuum assumption in cancellous bone, J. Biomech. 21 (1988) 269–275.

[40] R.S. Lakes, Dynamical study of couple stress effects in human compact bone, J. Biomech. Eng. 104 (1981) 6–11.

[41] H.C. Park, R.S. Lakes, Cosserat micromechanics of human bone: Strain redistribution by a hydration sensitive constituent, J. Biomech. 19 (53) (1986) 85–97.

[42] J.F.C. Yang, R.S. Lakes, Experimental study of micropolar and couple stress elasticity in compact bone in bending, J. Biomech. 15 (2) (1982) 91–98.

[43] S. Weiner, H.D. Wagner, The material bone: Structure-mechanical function relations, Annu. Rev. Mater. Sci. 28 (1998) 271–298.

[44] I. Jasiuk, Modeling of trabecular bone as a hierarchical material, Comput. Fluid Solid Mech. 1 (2) (2003) 1727–1728.

[45] M. Rubin, I. Jasiuk, The TEM characterization of the lamellar structure of osteoporotic human trabecular bone, Micron 36 (2005) 653–664.

[46] J.F.C. Yang, R.S. Lakes, Transient study of couple stress in compact bone torsion, J. Biomech. Eng. 103 (1981) 275–279.

[47] A. Yoo, I. Jasiuk, Modeling of trabecular bone as a couple stress continuum, Adv. Bioeng. ASME (2003) 41–42.

[48] A. Yoo, I. Jasiuk, Couple-stress moduli of a trabecular bone idealized as a 3D periodic cellular network, J. Biomech. 39 (2006) 2241–2252.

[49] J. Fatemi, F. Van Keulen, P.R. Onck, Generalized continuum theories: Application to stress analysis in bone, Meccanica 37 (4–5) (2002) 385–396.

[50] A. Papanicolopulos, A. Zervos, Continua with microstructure: Second gradient theory. Theory, examples and computational issues, Eur. J. Environ. Civ. Eng. 14 (8–9) (2010) 1031–1050.

[51] E.C. Aifantis, Strain gradient interpretation of size effects, Int. J. Fract. 95 (1999) 299–314, Eur. J. Mech. A, Solids 21 (3) (2002) 465–481.

[52] G.E. Exadaktylos, I. Vardoulakis, Microstructure in linear elasticity and scale effects: A reconsideration of basic rock mechanics and rock fracture mechanics, Tectonophysics 335 (2001) 81–109.

[53] P. Germain, La méthode des puissances virtuelles en mécanique des milieux continus, premiere partie, théorie du second gradient, J. Méc. 12 (2) (1973) 234–274.

[54] F. dell'Isola, P. Seppecher, The relationship between edge contact forces, double force and interstitial working allowed by the principle of virtual power, C. R. Acad. Sci. Paris, Ser. IIb 321 (1995) 303–308.

[55] F. dell'Isola, H. Gouin, P. Seppecher, Radius and surface tension of microscopic bubbles by second gradient theory, C. R. Acad. Sci. Paris, Ser. IIB 320 (1995) 211–216.

[56] F. dell'Isola, H. Gouin, G. Rotoli, Nucleation of spherical shell-like interfaces by second gradient theory: Numerical simulations, Eur. J. Mech. B, Fluids 15 (4) (1996) 545–568.

[57] F. dell'Isola, P. Seppecher, Edge contact forces and quasi-balanced power, Meccanica 32 (1997) 33–52.

[58] F. dell'Isola, G. Sciarra, S. Vidoli, Generalized Hooke's law for isotropic second gradient materials, Proc. R. Soc. A 465 (2107) (2009) 2177–2196.

[59] R.A. Toupin, Elastic materials with couple-stresses, Arch. Ration. Mech. Anal. 11 (1962) 385–414.

[60] S. Quiligotti, G. Maugin, F. dell'Isola, An Eshelbian approach to the nonlinear mechanics of constrained solid-fluid mixtures, Acta Mech. 160 (2003) 45–60.

[61] G. Sciarra, F. dell'Isola, N. Ianiro, A. Madeo, A variational deduction of second gradient poroelasticity I: General theory, J. Mech. Mater. Struct. 3 (3) (2008) 507–526.

[62] A. Luongo, A. Paolone, Perturbation methods for bifurcation analysis from multiple nonresonant complex eigenvalues, Nonlinear Dyn. 14 (1997) 193–210.

[63] A. Luongo, A. Paolone, Multiple scale analysis for divergence-Hopf bifurcation of imperfect symmetric systems, J. Sound Vib. 218 (3) (1998) 527–539.

[64] A. Luongo, A. Paolone, A. Di Egidio, Multiple time scales analysis for 1:2 and 1:3 resonant Hopf bifurcations, Nonlinear Dyn. 34 (2003) 269–291.

[65] A. Di Egidio, A. Luongo, A. Paolone, Linear and non-linear interactions between static and dynamic bifurcations of damped planar beams, Int. J. Non-Linear Mech. 42 (2007) 88–98.

[66] A. Alessandroni, F. dell'Isola, M. Porfiri, A revival of electric analogs for vibrating mechanical systems aimed to their efficient control by PZT actuators, Int. J. Solids Struct. 39 (2002) 5295–5324.

[67] U. Andreaus, F. dell'Isola, M. Porfiri, Piezoelectric passive distributed controllers for beam flexural vibrations, J. Vib. Control 10 (2004) 625.

[68] F. dell'Isola, S. Vidoli, Damping of bending waves in truss beams by electrical transmission lines with PZT actuators, Arch. Appl. Mech. 68 (1998) 626–636.

[69] E. Hamed, Y. Lee, I. Jasiuk, Multiscale modeling of elastic properties of cortical bone, Acta Mech. 213 (1–2) (2010) 131–154.

[70] D. Inglis, S. Pietruszczak, Characterization of anisotropy in porous media by means of linear intercept measurements, Int. J. Solids Struct. 40 (5) (2003) 1243–1264.

[71] J.Y. Rho, R.B. Ashman, C.H. Turner, Young's modulus of trabecular and cortical bone material: Ultrasonic and microtensile measurements, J. Biomech. 26 (2) (1993) 111–119.

[72] F. dell'Isola, A. Romano, On the derivation of thermomechanical balance equations for continuous systems with a nonmaterial interface, Int. J. Eng. Sci. 25 (1987) 1459–1468.

[73] F. dell'Isola, L. Rosa, C. Woźniak, A micro-structured continuum modelling compacting fluid-saturated grounds: The effects of pore-size scale parameter, Acta Mech. 127 (1998) 165–182.

[74] F. dell'Isola, M. Guarascio, K. Hutter, A variational approach for the deformation of a saturated porous solid. A second-gradient theory extending Terzaghi's effective stress principle, Arch. Appl. Mech. 70 (2000) 323–337.

[75] F. dell'Isola, L. Rosa, An extension of Kelvin and Bredt formulas, Math. Mech. Solids 1 (1996) 243–250.

[76] S. Forest, D.K. Trinh, Generalized continua and non-homogeneous boundary conditions in homogenization methods, ZAMM 91 (2011) 90–109.

[77] S. Forest, E.C. Aifantis, Some links between recent gradient thermo-elasto-plasticity theories and the thermomechanics of generalized continua, Int. J. Solids Struct. 47 (2010) 3367–3376.

[78] S. Forest, Milieux continus généralisés et matériaux hétérogènes, Les presses de l'Ecole des Mines, Paris, ISBN 2-911762-67-3, Avril 2006.

[79] F. dell'Isola, A. Romano, A phenomenological approach to phase transition in classical field theory, Int. J. Eng. Sci. 25 (1987) 1469–1475.

[80] C.Y. Wang, L. Feng, I. Jasiuk, Scale and boundary conditions effects on the apparent elastic moduli of trabecular bone modeled as a periodic cellular solid, J. Biomech. Eng., Trans. ASME 131 (12) (2009) 121008.

[81] R.D. Mindlin, Second gradient of strain and surface tension in linear elasticity, Int. J. Solids Struct. 1 (1965) 417–438.